Journal of Engineering for Gas Turbines and Power

Copy of e-mail Notification

Journal of Engineering for Gas Turbines and Power Published by ASME
Dear Author,
Congratulations on having your paper accepted for publication in the ASME Journal Program.
Your page proof is available in PDF format from the ASME Proof Download & Corrections site here:
http://115.111.50.156/jw/AuthorProofLogin.aspx?pwd=00f47ec569d2&CA=AS

Login: your e-mail address
Password: 00f47ec569d2

Please keep this email in case you need to refer back to it in the future.
You will need Adobe Acrobat Reader software to view the file. This is free software and a download link is provided when you log in to view your proofs.

Responsibility of detecting errors rests with the author. Please review the page proofs carefully and:
1. Answer any queries on the first page "Author Query Form"
2. Proofread any tables and equations carefully
3. Check to see that any special characters have translated correctly
4. Publication will not proceed until a response is received. If there are no corrections, a response is still required.

RETURNING CORRECTIONS:
Corrections must be returned using the ASME Proof Download & Corrections Submission Site (link above). You will be able to upload:
1. Annotated PDF
2. Text entry of corrections, with line numbers, in the text box provided
3. Additional files, if necessary.

SPECIAL NOTES:
Your Login and Password are valid for a limited time. Please reply within 48 hours.

Corrections not returned through the above website will be subject to publication delays. This e-proof is to be used only for the purpose of returning corrections to the publisher. If you have any questions, please contact: asme.cenveo@cenveo.com, and include your article no. (GTP-15-1314) in the subject line. This email should not be used to return corrections.

Approval of these proofs re-confirms the copyright agreement provision that all necessary rights from third parties for any copyrighted material (including without limitation any diagrams, photographs, figures or text) contained in the paper has been obtained in writing and that appropriate credit has been included.

Sincerely,
Mary O'Brien, Journal Production Manager

STATEMENT OF EDITORIAL POLICY AND PRACTICE

The Technical Committee on Publications and Communications (TCPC) of ASME aims to maintain a high degree of technical, literary, and typographical excellence in its publications. Primary consideration in conducting the publications is therefore given to the interests of the reader and to safeguarding the prestige of the Society.

To this end the TCPC confidently expects that sponsor groups will subject every paper recommended by them for publication to careful and critical review for the purpose of eliminating and correcting errors and suggesting ways in which the paper may be improved as to clarity and conciseness of expression, accuracy of statement, and omission of unnecessary and irrelevant material. The primary responsibility for the technical quality of the papers rests with the sponsor groups.

In approving a paper for publication, however, the TCPC reserves the right to submit it for further review to competent critics of its own choosing if it feels that this additional precaution is desirable. The TCPC also reserves the right to request revision or condensation of a paper by the author or by the staff for approval by the author. It reserves the right, and charges the editorial staff, to eliminate or modify statements in the paper that appear to be not in good taste and hence likely to offend readers (such as obvious advertising of commercial ventures and products, comments on the intentions, character, or acts of persons and organizations that may be construed as offensive or libelous), and to suggest to authors rephrasing of sentences where this will be in the interest of clarity. Such rephrasing is kept to a minimum.

Inasmuch as specific criteria for the judging of individual cases cannot, in the opinion of the TCPC, be set up in any but the most general rules, the TCPC relies upon the editorial staff to exercise its judgment in making changes in manuscripts, in rearranging and condensing papers, and in making suggestions to authors. The TCPC realizes that the opinions of author and editor may sometimes differ, and hence it is an invariable practice that no paper is published until it has been passed on by the author. For this purpose page proofs of the edited paper are sent to the author prior to publication in a journal. Changes in content and form made in the proofs by authors are followed by the editor except in cases in which the Society's standard spelling and abbreviation forms are affected.

If important differences of opinion arise between author and editor, the points at issue are discussed in correspondence or interview, and if a solution satisfactory to both author and editor is not reached, the matter is laid before the TCPC for adjustment.

Technical Committee on Publications and Communications (TCPC)
Reviewed: 05/2012

AUTHOR QUERY FORM

ASME SETTING THE STANDARD	**Journal: J. Eng. Gas Turbines Power** **Article Number: GTP-15-1314**	**Please provide your responses and any corrections by annotating this PDF and uploading it to ASME's eProof website as detailed in the Welcome email.**

Dear Author,

Below are the queries associated with your article; please answer all of these queries before sending the proof back to Cenveo. Production and publication of your paper will continue after you return corrections or respond that there are no additional corrections.

Location in article	Query / Remark: click on the Q link to navigate to the appropriate spot in the proof. There, insert your comments as a PDF annotation.
AQ1	As per journal style three or fewer letters acronyms are not allowed in the title; therefore, we have replaced the acronym CFD with the spelled out definition.
AQ2	Please provide postal code for affiliations.
AQ3	Please verify the language edits made across the article.
AQ4	Please verify the deletion of the sentence "From their results…" Kindly advice.
AQ5	Please provide publisher name and location for Ref. 3.
AQ6	There were two equations numbered (3, 4, and 5) in your paper, hence we have changed the repeated number to Eqs. (7, 8, and 9) and renumbered all subsequent equations accordingly. Please check all renumbering and update the citations in the text as needed.
AQ7	In Ref. 20 Year should be changed. Please check and confirm.
AQ8	Please provide DOI for Refs. 15, 21, 26 and 27.

Thank you for your assistance.

AQ2 **Alessio Suman**[1]
Dipartimento di Ingegneria,
Università degli Studi di Ferrara,
Ferrara ■, Italy

Rainer Kurz
Solar Turbines Incorporated,
San Diego ■, CA
AQ1

Nicola Aldi
Dipartimento di Ingegneria,
Università degli Studi di Ferrara,
Ferrara ■, Italy

Mirko Morini
Dipartimento di Ingegneria Industriale,
Università degli Studi di Parma,
Parma ■, Italy

Klaus Brun
Southwest Research Institute,
San Antonio, TX ■

Michele Pinelli
Dipartimento di Ingegneria,
Università degli Studi di Ferrara,
Ferrara ■, Italy

Pier Ruggero Spina
Dipartimento di Ingegneria,
Università degli Studi di Ferrara,
AQ3 Ferrara ■, Italy

Quantitative Computational Fluid Dynamics Analyses of Particle Deposition on a Subsonic Axial Compressor Blade

In literature, there are some studies related to the fouling phenomena in transonic compressors, but, in industrial applications (heavy-duty compressor, pump stations, etc.) the subsonic compressors are widespread. It is of great interest to the manufacturer to discover the fouling phenomenon related to this type of compressor. This paper presents three-dimensional numerical simulations of the microparticle ingestion on a subsonic axial compressor rotor carried out by means of a commercial computational fluid dynamic code. Particle trajectory simulations use a stochastic Lagrangian tracking method that solves the equations of motion separate from the continuous phase. The number of particles, sizes, and concentrations are specified in order to perform a quantitative analysis of the particle impact on the blade surface. In this paper, the particle impact pattern and the kinematic characteristics (velocity and angle) of the impact are shown. Both of the blade zones affected by particle impact and the blade zones affected by particle deposition are analyzed. The particle deposition is established by using the quantity called sticking probability (SP). The SP links the kinematic characteristics of particle impact on the blade with fouling phenomenon. The results show that microparticles tend to follow the flow by impacting at full span with a higher impact concentration on the leading edge (LE). The suction side (SS) is affected only close to the LE and, at the hub, close to the trailing edge (TE). Particular fluid-dynamic phenomena such as separation, stagnation, and tip leakage vortex strongly influence the impact location of the particles. The kinematic analysis showed a high tendency of particle adhesion on the SS, especially for smaller particles for which the fluid dynamic phenomena play a key role regarding particle impact velocity and angle. [DOI: 10.1115/1.4031205]

Introduction

Heavy-duty axial compressors (used in gas turbines and/or in industrial processes such as compressor stations and pump stations) ingest a large amount of air during their operation. The quality and purity of the air entering the compressor is a significant factor in the performance and life of the gas turbine.

The air contains and carries a large number of particles that, through mechanisms not fully understood, stick to the blade surfaces and determine fouling phenomenon [1]. Evaluation of fouled compressors has revealed contamination both on the SS and the pressure side (PS) of the compressor blades [1].

Particle adhesion on the blade surfaces is a complex phenomenon that includes many aspects (materials, surface conditions, particle size, and impact dynamic). Particle sticking on blade surfaces results in an increase in the thickness of the airfoil and the surface roughness. Both of these events change the flow-path inside the passage vanes. Fouling is recoverable by water washing but the real issue is the rate of fouling, which determines the frequency of washing. Since the engine needs to be shut down for washing, it will not generate revenue for a day [2]. In order to minimize the performance loss, a filtration system that can limit the ingestion of contaminants by the power unit is required. For industrial gas turbines, highly effective filtration systems exist [3] that are effective in removing particles smaller than 0.1 μm and larger than 2.0 μm. For these reasons, erosion is not a problem, and only the fouling phenomenon represents the big issue in industrial applications.

After the particle deposition to the blade surface, the only method for recovering the performances of the compressor is washing operation [1]. Experimental results reported in Ref. [4] demonstrated that the process of washing was assumed to recover the output power until 99.5%. Fouling can be removed by offline washing and slowed down by online washing. The decision to shut the engine down for offline washing is a balance between lost production due to the lower power versus the lost production for shutting the engine down for a certain amount of time.

In this article, an extended study on particle ingestion with diameters close to 1 μm was carried out. The computational strategy and the methodology used for the data postprocess reported in Refs. [5,6] are applied to a subsonic rotor compressor. Even if, in the last decade, manufacturers have been oriented to the development of the transonic axial compressor, the subsonic stages are commonly used for heavy-duty industrial applications, thanks to their very high reliability and relatively restrained cost (maintenance and recovery).

Literature Review

Fouling phenomenon can be described by the following three phases: (i) transport of the contaminants by the airflow stream, (ii) contact and adhesion of the first particle with the surface, and (iii) repeated adhesion of the following particles. A comprehensive study of the fouling phenomenon must contain the resolution of the three phases of adhesion and/or rebound.

The interaction between two bodies, with or without the action of an external force, has been a subject of study since the

[1]Corresponding author.

Contributed by the Turbomachinery Committee of ASME for publication in the Journal of Engineering for Gas Turbines and Power. Manuscript received July 15, 2015; final manuscript received July 22, 2015; published online xx xx, xxxx. Editor: David Wisler.

Nineteenth Century. In 1882, Hertz [7] studied and described the normal impacts of sphere–sphere and sphere–surface. In his studies, the yield load, and therefore the body deformation strongly influenced the result of the impact. Over the last decades, other research has been realized in order to better understand the phenomena during particle impact. In 1971, Johnson et al. [8] demonstrated that even if there is not an external force maintaining two bodies in contact, a force greater than zero is necessary to separate it. Subsequently, in 1990, Wall et al. [9] highlighted that plastic deformation is a significant component of energy loss at all impact velocities and in 1998, Thornton and Ning [10] demonstrated that for a high impact velocity the energy interface does not affect the rebound characteristics.

Unfortunately, most of the models and the results reported in literature do not provide a full understanding of the adhesion phenomena which are responsible for the fouling mechanism. This limit is largely due to: (i) different particle sizes, (ii) different material characteristics (some particle materials do not show the elastic yield limit), and (iii) different impact velocities.

Therefore, by using the analytical model it is impossible to predict the amount and localization of deposits on the blade surfaces. Some attempts in the fouling investigations are realized by experimental tests. Among others, Parker and Lee [11] reported a study of fouling patterns on blades caused by an ingestion of submicron particles (from 0.13 μm to 0.19 μm).

Nevertheless, the experimental applications related to the fouling phenomenon and the results as a consequence are affected by numerous problems summarized as follows: (i) actual conditions of the contaminants and the work environment of the compressor, (ii) size of the experimental test bench, in particular even if the cascade and the velocities are scalable, the particle dimensions are not scalable and their ratio with respect to the cascade and the velocities must be respected, (iii) rotational velocity of the cascade (neglected in nearly all experimental apparatus) influences the dynamic and the kinematic characteristics of the particle impact, (iv) the modification of the interface between the particle and the blade in order to accelerate the fouling process limiting the validity of the results, and finally, (v) the lack of the particle count, in particular the lack of the ratio between the injected particles and the stuck particles. For these reasons, it is possible to understand the mechanisms that determine the fouling phenomenon not only by using experimental applications.

An innovative approach may be represented by the match between the experimental results and computational fluid dynamics (CFD) results. In this way, the problems in the experimental tests mentioned above can be solved by using the numerical CFD simulations. Thus, interdisciplinary research can represent the new frontier for a considerable upgrade in fouling investigation. Some very interesting results and analysis of microparticle adhesion can be found in astrophysics research (preplanetary dust). The uniqueness and usefulness of these studies is that the particle velocities, materials, and dimensions are in the same range as those responsible for the fouling phenomenon.

Interesting results are reported in Refs. [12–14]. In particular, in Ref. [12], the authors reported an experimental evaluation of perfectly spherical and irregular particles impacting a smooth surface (smooth as the particle surface). Different combinations of particle size and materials have been tested. The particle diameters are very close to 1 μm and in some cases the experiments were conducted with submicrometric particles. The results reported in these works refer to a particular quantity called SP. The SP was evaluated by a statistical approach which emphasizes that particle impacts are different from each other and, in order to provide a macroscopic evaluation of the results, a statistic/probabilistic approach is the best way. The SP is reported as a function of particle impact normal velocity. From these analyses, it is easy to understand that for the total comprehension of particle impact behavior, *how* the contaminants hit the blade surface must be known. In this context, the word *how* refers to the impact velocity and the impact angle for each particle.

For these reasons, the coupled approach experimental test-CFD simulation can represent the best strategy to link the particle kinematic characteristics discovered through the numerical simulations and the adhesion characteristics discovered through experimental tests.

Some CFD studies related to particle tracking in the axial compressor are reported in the literature [15–17], but the attention is only referred to the erosion phenomena and not to fouling issues. The particle diameters in fact are comprised of in the range (10–1000) μm. The deposition phenomena (that cause a fouling issue) are related to submicro particles and the CFD strategy must be tailored to these specific sizes in order to avoid the nonrealistic representation of the particle trajectories, in particular, close to the walls.

Suman et al. [5,6] reported the coupling of the experimental results related to particle sticking and the CFD results related to particle trajectories and dynamic characteristics. The authors have highlighted the behavior of particle ingestion by a transonic rotor. The transonic compressor has a greater manufacturer interest, particularly for use with high loaded heavy duty power units. The principle results reported in Refs. [5,6] are:

—increasing the particle diameter increases the number of particles that impact a transonic blade;
—increasing the particle diameter, the PS is more contaminated than the SS;
—in the PS, the ratio between the number of stuck particles and the injected particles is almost independent with respect to the particle diameter;
—in the SS, the ratio between the number of stuck particles and the injected particles is dependent on the particle diameter and follows the decreasing trend of the ratio between the particles that impact the SS and the injected particles;
—the three-dimensional fluid dynamic phenomena such as a separation and tip leakage vortex strongly influence the particle impact pattern and the adherence conditions.

In this paper, the authors will apply the same strategy to a subsonic rotor with performances which significantly differ from those reported in Refs. [5,6]. The subsonic compressor is widespread in compressor stations and in more industrial applications. Therefore, this paper is developed according to the following points:

—validation of the numerical models by using the experimental and numerical data reported in literature,
—simulation of the ingestion of a fine powder characterized by different particle diameters (from 0.15 μm to 2.00 μm);
—quantitative and sensitivity analysis of the particle impact and evaluation of the air contaminant concentration around the blade surfaces;
—highlighting the kinematic characteristics of the particles that impact on an axial compressor blade. Particular attention is given to particle impact velocity and particle impact angle for the PS and SS;
—an analysis of the normal and tangential velocity component in order to define the relative impact kinematic characteristics between blade and particles;
—estimates of the SP up to 1 μm particle

Diameter in order to define the preferable deposition zones on the blade as a function of the particle diameter.

Numerical Model

The numerical simulations were carried out by means of the commercial CFD code ANSYS FLUENT 13.0. The standard k–ε turbulence model with a standard wall function (STW) was used. All the simulations were performed in a steady multiple frames of reference by using a frozen rotor interface. The numerical domain is composed by three domains: two stationary domains (inlet and outlet duct) and one rotating domain (rotor).

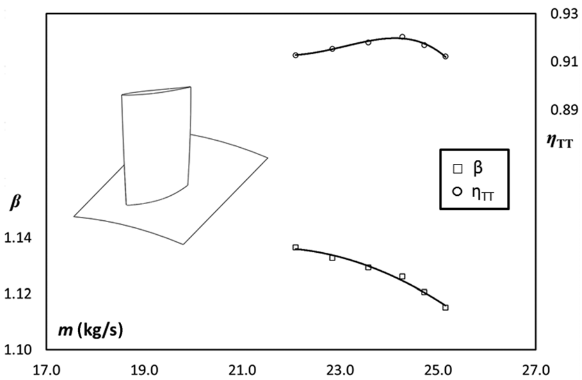

Fig. 1 Performance: compression ratio and efficiency

Continuum Phase. The subsonic rotor is the first stage of a multistage axial compressor used in an industrial application. It is composed of 31 blades but only a single passage vane was modeled. The hub to tip ratio is equal to 0.739, while the tip clearance is 0.382 mm (0.45% of the blade span). The subsonic rotor is studied at the nominal rotational speed equal to 6054 rpm and the peripheral velocity at the blade tip is equal to 206 m/s. A multiblock hexahedral grid with a total number of 1,007,800 elements was used. Regarding the near walls, the nodes are positioned in such a way that the values of y^+ are within 5–71. The inlet surface mesh has every single element with the same size in order to guarantee a uniform node distribution on the surface. The uniform distribution of grid nodes allows the realization of a uniform particle injection from this surface. An inlet surface of 2596 hexahedral elements was created. The inlet total pressure and total temperature were imposed at 101,325 Pa and 288.15 K, respectively. An average static pressure p_2 was imposed at the outflow boundary, both in the near-choked flow region and in the near-stall region. The outflow pressure was progressively increased in order to perform the entire performance trends. The performance trends in terms of total pressure ratio β and the total-to-total efficiency η_{TT} are reported in Fig. 1. Figure 1 also reports the blade shape of the subsonic rotor.

Discrete Phase. In this paper, the solution approach is based on a mathematical model with Eulerian conservation equations in the continuous phase and a Lagrangian frame to simulate a discrete second phase. In this approach, the airflow field is first simulated, and then the trajectories of individual particles are tracked by integrating a force balance equation on the particle.

The force balance is comprehensive of: inertia, drag, and buoyancy terms. In the force balance, there are two contributes due to the shear stress and diffusion called Saffman's lift force and Brownian force but these two contributes become important in very few cases. In this paper, only the Brownian term was neglected. An extensive description of the force balance can be found in Ref. [5].

For the particle–wall interaction boundary conditions, the following conditions have been adopted: (i) ideal adherence condition (named *trap*) on the blade surfaces and (ii) nonadherence condition (named *reflect*) on the hub and shroud surfaces. These conditions allow the evaluation of where and how the contaminants encountered the blade surface for the first time, avoiding the introduction of inaccuracies due to the use of bounce models not fully representative of the real conditions. The authors have implemented specific functions and restitution coefficients for the near-wall particle behavior. The model functions are defined in agreement with Ahlert's model [18] and Forder's coefficients [19]. In general applications, restitution coefficients could depend on (i) impact velocity, (ii) pressure, and (iii) temperature [20]. In this case, only the velocity could represent an obstacle through the correct representation of the particle bounce. The restitution coefficients used in this work were obtained from the Forder's work (Forder et al., 1998) in which an oilfield control valve was studied with a flow velocity almost equal to 80 m/s. This value of velocity added to the locations where the restitution coefficients are imposed determines the validity of the assumption to consider the restitution coefficients independent from the velocity. Regarding the variation of the restitution coefficients due to the presence of a third material at the interface between surface and particle (such as liquid water due to the combination of high humidity > 60% and the inlet depression), data are not available in literature. The authors in Ref. [12] pointed out that the presence of hydrophobic silane coating did not change the collisional behavior with respect to another test in which the surface was only cleaned with alcohol and subsequently dried with pressurized air. Generally, in the actual compressors, the presence of a third substance (such as oil, grease, etc.) on the blade surface could decrease the restitution coefficients (and then increase the SP) of the particle, but, at the moment, there are no specific studies that allow the quantification of this effect. More details regarding particle–wall interaction can be found in Ref. [5].

The density particle is equal to 2560 kg/m^3 and the variation of the particle diameter, d_p, is in the range of (0.15–2.00) μm, while the Stokes number (Eq. (1)) (calculated at the inlet of the numerical model) is in the range of 0.0003–0.05

$$\mathrm{St} = \frac{\rho_p d_p^2}{18\mu}\frac{U_1}{d_h} \tag{1}$$

All particles are spherical and nondeformable.

All the analyses refer to injections having particles with the same diameter, the same material, and thus characterized by the same Stokes number. On the other hand, the total flow rate of the discrete phase, m_p, is linked to the work environment of the compressor and the efficiency of the filtration system. For this reason, a different value of total flow rate of contaminants was imposed at the inlet of the compressor. In order to achieve the uniform particle concentration assumption, particles were released at the same velocity as the freestream ($\approx$ 140 m/s) in correspondence with the inlet surface, far from the rotor about 1.5 chord. It is assumed that the particles will not affect the fluid flow (one-way coupling) as the volume fraction of the particles was very low ($\ll$10%). All injections take place on a previously solved flow field, with the compressor operating at the best efficiency point. All results presented in this paper were obtained from convergent simulations, with a variation of the residues of the motion and turbulent equations close to zero and all lower than 10^{-4}. The injection data are summarized in Table 1 (more details can be found in Ref. [5]).

Table 1 Characteristics of the injections

Case	1	2	3	4	5	6
Particle diameter, d_p (μm)	0.15	0.25	0.50	1.00	1.50	2.00
Stokes number, St	3×10^{-4}	8×10^{-4}	3×10^{-3}	1×10^{-2}	3×10^{-2}	5×10^{-2}
Nondim. relax. time, τ^+	1	3	13	52	117	209
Filtration eff., η_f (%)	61	60	65	85	96	99
Mass flow rate, m_p (kg/s)	9.8×10^{-7}	4.7×10^{-6}	3.3×10^{-5}	1.1×10^{-4}	1.0×10^{-4}	6.0×10^{-5}

Particle Turbulent Dispersion. The dispersion of particles in the fluid phase can be predicted by using a stochastic tracking model. This investigation used the discrete random walk (DRW) model to simulate the stochastic velocity fluctuations in the airflow. The number of trajectories was selected in order to satisfy the statistical independence since the turbulent dispersion is modeled based on a stochastic process. Each analysis of three different injections with 1100 trajectories was carried out.

Through the use of k–ε turbulence model with STW, there is an isotropic treatment of the turbulence near the wall and this implies, in the case where the values of y^+ are less than 5, that both the streamwise mean velocity and the turbulence kinetic energy will be overestimated. More details can be found in the work of Tian and Ahmadi [21]. In this paper, as mentioned above, the values of y^+ do not drop below 5. Tian and Ahmadi [21] highlighted the effect of a different turbulence model on the velocity deposition for particles in a horizontal and vertical tube. In order to investigate the relationship between the turbulence models, mesh refinement close to the wall and particle dimensions in greater detail, it is possible to calculate the nondimensional particle relaxation time τ^+ defined as

$$\tau^+ = \frac{(\rho_p/\rho) d_p^2 u_t^2}{18\nu^2} \tag{2}$$

where the u_t is the shear velocity defined as

$$u_t = \sqrt{\frac{\tau_w}{\rho}} \tag{3}$$

and τ_w is the wall shear stress. Tian and Ahmadi [21] have shown that the k–ε turbulence model with STW overpredicts the deposition velocity for particles in a Brownian ($\tau^+ < 10^{-2}$) and transition ($10^{-2} < \tau^+ < 10$) region and it does not allow the estimation of the real trend of the particle velocity deposition. For the inertial ($\tau^+ > 10$) region, the k–ε STW turbulence model overpredicts the deposition velocity but in a minor way compared to the other regions and the trend of the deposition velocity curve is in agreement with the other results. As can be seen in Table 1, the nondimensional particle relaxation time τ^+, defined by Eq. (2), is in the range of 1–209 which corresponds to the transition and inertial region. However, the values in the transition region are close to the inertial region and thanks to the analyses mentioned above (values of y^+ and τ^+), the k–ε STW turbulence model used for all the analyses was considered suitable for studying the real deposition phenomenon that occurs in the axial compressors under investigation.

Results

Capture Efficiency. In this section, the analysis of the particle impact on the blade surface is shown. Only a portion of particles injected from the inlet surface of the numerical model impacts on the blade surface, and due to the imposed surface condition (ideal-adherence), the contact results in a permanent adherence. For comparison among the studied cases, the ratio η_{hit} can be used. The η_{hit} is defined as the ratio between the number of particles that hit the blade and the total number of injected particles. The trend of the η_{hit} as a function of the particle diameter d_p is reported in Fig. 2.

From Fig. 2, it is possible to observe that the percentage of the particles that hit the blade surface increases with the diameter of the particles (solid line), with a law quite different from the variation of the Stokes number (dashed line). The same results not shown for the sake of brevity is obtained by comparing these two trends with the trends of the nondimensional particle relaxation time τ+, defined in Eq. (2). The increase of impacting particles with increasing nondimensional relaxation time is consistent with the indications given by Tian and Ahmadi [21]. In Fig. 2, the total number of particles injected and the absolute number of impacting particles on the blade surface are also reported for all studied cases.

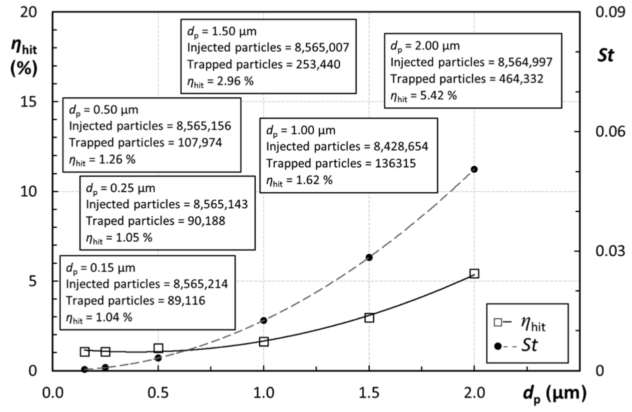

Fig. 2 Capture efficiency η_{hit} and Stokes number St versus particle diameter d_p

Due to the wall–particle interaction settings, the particles do not stick to the hub and shroud. Particles bounce on these surfaces following the rules imposed by the restitution coefficients. In Table 2, the global count of the bounces is reported. The values of N_b represent the number of particles that bounce on the hub or shroud, the values of n_b represent the ratio between the number of particles that bounce on the hub or shroud and the total number of injected particles, and finally, the values of b represent the average number of bounces of each particle.

It can be noticed that the number of bouncy particles increases with the increase of particle diameter but, conversely, the number of average bounces decreases with the increase of particle diameter. This implies that for the smaller diameters, the particles that hit the blade may have had more frequent multiple impacts on the hub or shroud before the impact with the blade. Thus, the smaller particles could have a better chance of sticking to the hub or shroud surface compared to the bigger ones. However, this phenomenon is related to a much smaller number of particles compared to the number of injected particles (less than 1.00%) and does not influence the overall results.

Particle Concentrations. By using the quantity defined as discrete phase model (DPM) concentration χ_{DPM}, it is possible to calculate the contaminant concentration kg/m^3 on a specific surface. The χ_{DPM} allows the combined effects between the trajectories of the particles and the total mass flow rate to be highlighted. In the present paper, the χ_{DPM} allows the evaluation of the combined effects of: (i) the particle trajectories, (ii) the contamination intensity of the working compressor place χ, and (iii) the filtration efficiency η_f. The selected surface to evaluate the χ_{DPM} was obtained

Table 2 Particles bounces on the hub and shroud

	Hub			Shroud		
d_p (µm)	N_b	n_b (%)	b	N_b	n_b (%)	b
0.15	40,551	0.47	4.1	47064	0.52	4.5
0.25	41,133	0.48	4.1	47,064	0.55	4.6
0.50	46,053	0.54	3.7	56,208	0.66	4.5
1.00	41,730	0.50	2.1	5,6478	0.67	3.0
1.50	34,143	0.40	1.2	53,241	0.62	2.2
2.00	28,659	0.33	0.7	53,205	0.62	1.8

by a transformation of the blade surface. The new surface was positioned at a constant distance from the blade surface of 50 μm for each point. In this way, it is possible to evaluate the presence of contaminants in the portion of fluid that is located very close to the blade surface. Figure 3 shows the contour plot of χ_{DPM} on the transform surface for PS and SS of the blade. From Fig. 3, it is possible to notice that:

—The peak of the contaminant concentration is found in correspondence to the LE.
—The PS is more contaminated than the SS.
—The injections with the smallest particles ($d_{\mathrm{p}} = 0.15\,\mu$m and $d_{\mathrm{p}} = 0.25\,\mu$m) show a more distributed contaminant concentration on the PS. The contaminant concentration in the corner region close to TE in the SS is clearly visible.
—The injections with the largest particles ($d_{\mathrm{p}} = 2.00\,\mu$m) show a relevant concentration of contaminants only on the PS and in a blade portion close to the LE in SS.

These distributions are in line with those reported in literature regarding (i) fouling characterized by particles with dimensions less than 2 μm [1] and (ii) erosion of rotor blades which is characterized by larger particles [17]. In fact, the fouling phenomenon is characterized by a wider distribution of the particle on the blade surfaces with respect to erosion, which shows a higher percentage of impacts on the PS and LE than on the SS.

The DPM concentration shown in Fig. 3 refers to one of the three runs. In fact, as mentioned above, every case was repeated for three different runs. The values obtained for the three runs are very close to each other and $\bar{\chi}_{\mathrm{DPM}}$ represents the average value of the weighted-area average value of DPM of each run (as reported in Ref. [5]). From the $\bar{\chi}_{\mathrm{DPM}}$, the ratio H can be defined as

$$H = \frac{\bar{\chi}_{\mathrm{DPM}}}{\chi M_p (1 - \eta_{\mathrm{f}})} \quad (4)$$

This represents the dimensionless index of the compressor's capacity to concentrate the contaminants in the vicinity of the blades. This ratio is a representative index of a real fouling condition in which the compressor operates. In fact, from this index it is possible to link the characteristics of (i) the amount of contaminants, (ii) the type of contaminants, (iii) the filtration efficiency, and (iv) the flow pattern inside the axial compressor. The most severe fouling condition at the best efficiency point of this subsonic rotor is case 6 which has a fouling index equal to 0.39, for which all four (i)–(iv) of the aforementioned characteristics determine the highest value of the index. This value is an order of magnitude less than those reported for a transonic rotor [5].

Particle Impact Locations. In this section, the analysis of the results refers to the impact location of the particles on the blade surface. Theoretically, zones with a high number of impacts will be more affected by the fouling phenomena, but actually the fouling phenomena depend on the sticking characteristic of the particles. A comprehensive analysis on the sticking characteristics and real fouling phenomena on the blade surface are reported in the following paragraphs.

Figure 4 reports the trends of the impacting particles on the blade (for both sides) for all the particle diameters: (i) the η_{hit} values reported for the pressure side $\eta_{\mathrm{hit,PS}}$ and suction side $\eta_{\mathrm{hit,SS}}$ refer to the percentage of particles that hit the PS or SS compared to the total number of injected particles while (ii) the η_{side} values, reported in pie charts, represent the percentage of particles that hit

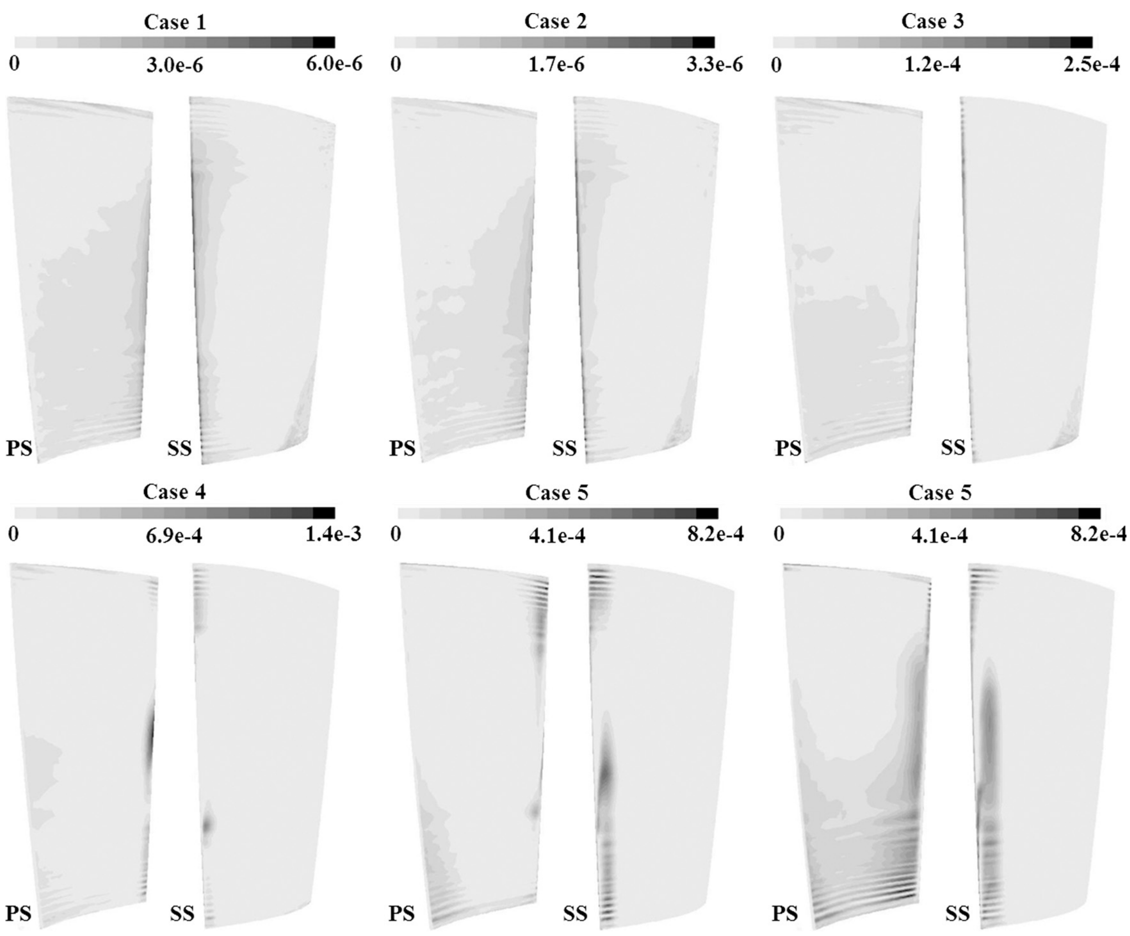

Fig. 3 DPM concentrations (kg/m^3), PS, and SS

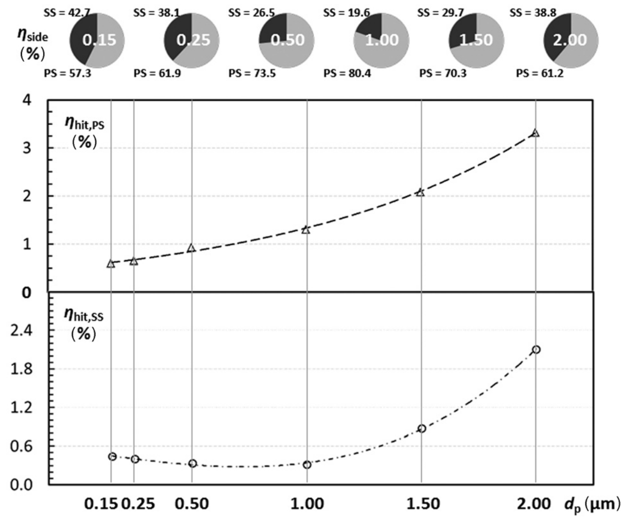

Fig. 4 Particle impact distributions, PS and SS

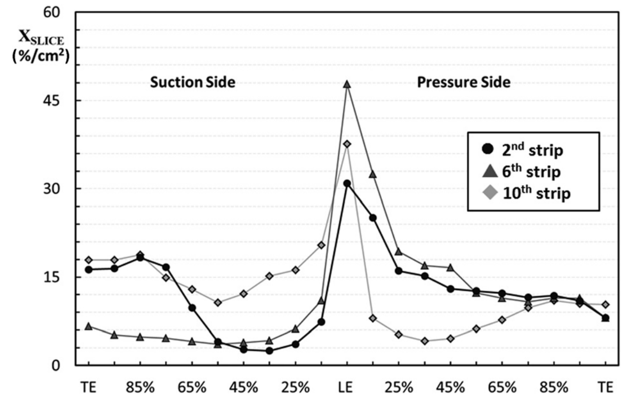

Fig. 6 Particle distributions X_{SLICE}, second, sixth, and tenth strip, case 1

the blade on the PS or SS compared to the total number of particles that hit the blade.

From the analysis of Fig. 4, it can be seen that by increasing the particle diameter, the number of particles that hit the PS increases. In the SS, the number of particles that hit the blade decreases to $d_p = 1.00\,\mu$m, while the number of impacts that takes place on the SS increases from $d_p = 1.00\,\mu$m to $d_p = 2.00\,\mu$m. The particles that hit the SS are especially concentrated at the LE of the blade as mentioned above. These overall results are directly related to the fluid dynamic phenomena that influence the flow field inside the rotor. In particular, two phenomena are reported in Fig. 5: (i) three-dimensional vortex at the rear part of the airfoil in the SS (due to the separation) drags the contaminants into the vicinity of the hub and (ii) the tip leakage vortex (due to tip gap) at the blade tip drags the particles from the PS to SS generating the presence of impacts on both sides of the blade. In the Appendix, an overall representation of the impact zone is reported.

From a fouling point of view, the most interesting results refer to the cases with the smaller particles. For these cases in fact, even if the number of particles that hit the blade surface is the smallest (see Fig. 4), the particles are present both in the PS and SS. For this reason, a significant and detailed analysis of the impact locations on the blade surface for case 1 ($d_p = 0.15\,\mu$m) is conducted. Thanks to a very fine discretization of the blade surface obtained through the use of 11 divisions (strips) along the spanwise direction, and 12 divisions (slices) along the chordwise direction, it is possible to clearly represent the deposits on the blade surface. In Fig. 6, concerning the second, sixth, and tenth strips (14%, 50%, and 86% of the blade span, respectively) the impact patterns along the chord for a specific strip can be noted. The quantity used in Fig. 6, X_{SLICE}, is defined as

$$X_{SLICE} = \left[\frac{N^\circ \text{ impacts @slice}}{N^\circ \text{ impacts @strip}} 100\right] \frac{1}{A_{\text{SLICE}}} \tag{5}$$

referring to the amount of impacts in a single slice obtained by a chordwise division of the strip with respect to the total number of particles that impact the entire considered strip. This quantity allows the representation of the results in general form and is very useful for comparative analyses. The quantity A_{SLICE} refers to the area of the slice obtained by a chordwise division of the strip. The adopted chordwise division is reported in abscissa for each distribution.

From Fig. 6, the high percentage of impacts on the LE can be noted which, in relative terms to the impacts on the strip, reaches a peak for the sixth strip (i.e., at midspan). A similar phenomenon can also be found in the experimental measurements reported by Parker and Lee [11] where the authors provided some deposition tests for a turbine blade.

The strip at midspan (sixth strip) shows a more uniform impact distribution on the blade surface, affecting the SS more than the PS. For the other two strips the impact distribution is quite different. For the second strip (close to the hub), the impact distribution in the SS shows an increment from 50% of the airfoil chord. The same phenomenon, even if smoother, can be noticed for the tenth (close to the blade tip), while in the PS the decreasing trend for the tenth strip shows an increment from 50% of the airfoil chord.

These impact patterns show that there is not a blade area completely free from particle impact and, as a consequence, the blade surface could be completely affected by the deposits. As reported in Ref. [22], clearance vortex due to the tip gap (close to the shroud) and corner vortex (close to the hub) determines three-dimensional flow structure of the flow field inside an axial compressor. In a three-dimensional flow field, secondary flows, driven by the flow through tip clearances and the imbalance between the pressure field and the kinetic energy of the air in the boundary layer,

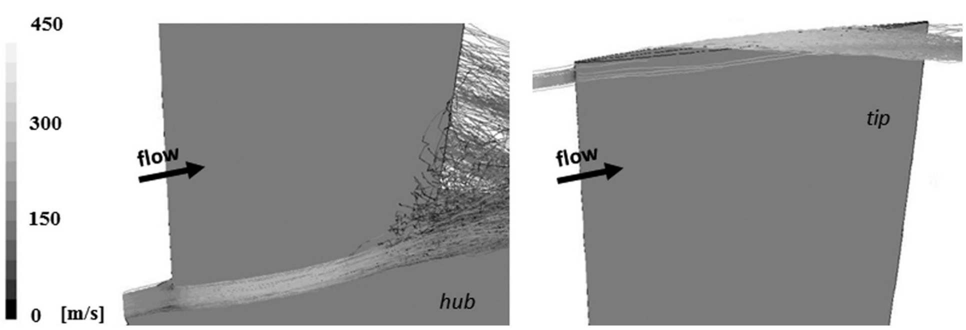

Fig. 5 Particle trajectories at the hub and at the blade tip, SS, case 2

have to be considered in the particle impact/deposition analysis. This means in particular, that particles can be deposited in places that would not be reachable for particles in two-dimensional flow.

In order to establish which particles are dangerous from a fouling point of view, the following analyses will be related to (i) impact velocity, (ii) impact angle, and finally (iii) SP. As mentioned above, the particle impact becomes adhesion only under specific conditions related to material and kinematic impact characteristics.

Impact Velocity. The first analysis is related to the particle impact velocity v_i. The modules of the particle impact velocity are reported in Fig. 7. The velocity values refer to the vector sum of the three velocity components u along the coordinate axes x, y, and z at the impact point on the blade surface.

In Fig. 7, three representative strips are reported: 2nd, 6th, and 11th (14%, 50%, and 95% of the blade span blade, respectively) divided into PS and SS. Each dot on the graph corresponds to the impacting particle on the blade. From Fig. 7 it can be noticed that:

—the impact velocity increases with the height of the blade and this phenomenon is due to the peripheral velocity;
—the lowest impact velocity can be found on the LE and on the TE of the SS;
—the highest impact velocity can be found on SS, in particular on the first part of the airfoil chord;

On the PS, the velocity trend is very similar for all the strips. At the LE and TE, the particles reach the peak of impact velocity while in the midchord the impact velocity reaches a minimum.

The analysis of Fig. 7 shows that the particle impact velocity is very different on the same side of blade. This difference is due to the shape of the blade (e.g., the blade height) and to the fluid dynamic phenomena: flow separation and tip leakage vortex. The flow separation influenced the particle impact velocity on the SS for the strips close to the hub. In particular at the second strips, the last part of the airfoil chord is affected by particles with a very low impact velocity. Flow separation in the corner region of the blade passage is common in axial compressors, as reported by Gbadebo et al. [23]. The tip leakage vortex due to the blade tip gap (0.382 mm, 0.45% of the blade span) influenced the particle impact at the top of the blade. As shown for the SS in Fig. 7, the rear part of the airfoil chord is impacted by particles with a very different impact velocity with respect to those in the other strips. The rear part of the airfoil chord of the 11th strip is impacted at the same time by particles with low and high impact velocities. The particles with the highest impact velocity are the particles dragged by the tip leakage vortex from the PS to the SS. In this specific case, the wall condition imposed on the blade surface (trap) determines a smaller amount of particles that are dragged from the PS to the SS. Under real conditions, some particles bounce off the PS and could reach the other side of the blade through the tip gap.

Impact Angle. As can be seen from the previous analyses, the particle impact velocity changes from the hub to the shroud, from the PS to the SS and along the airfoil chord. As mentioned above, particle adhesion is due to a combination of a number of effects,

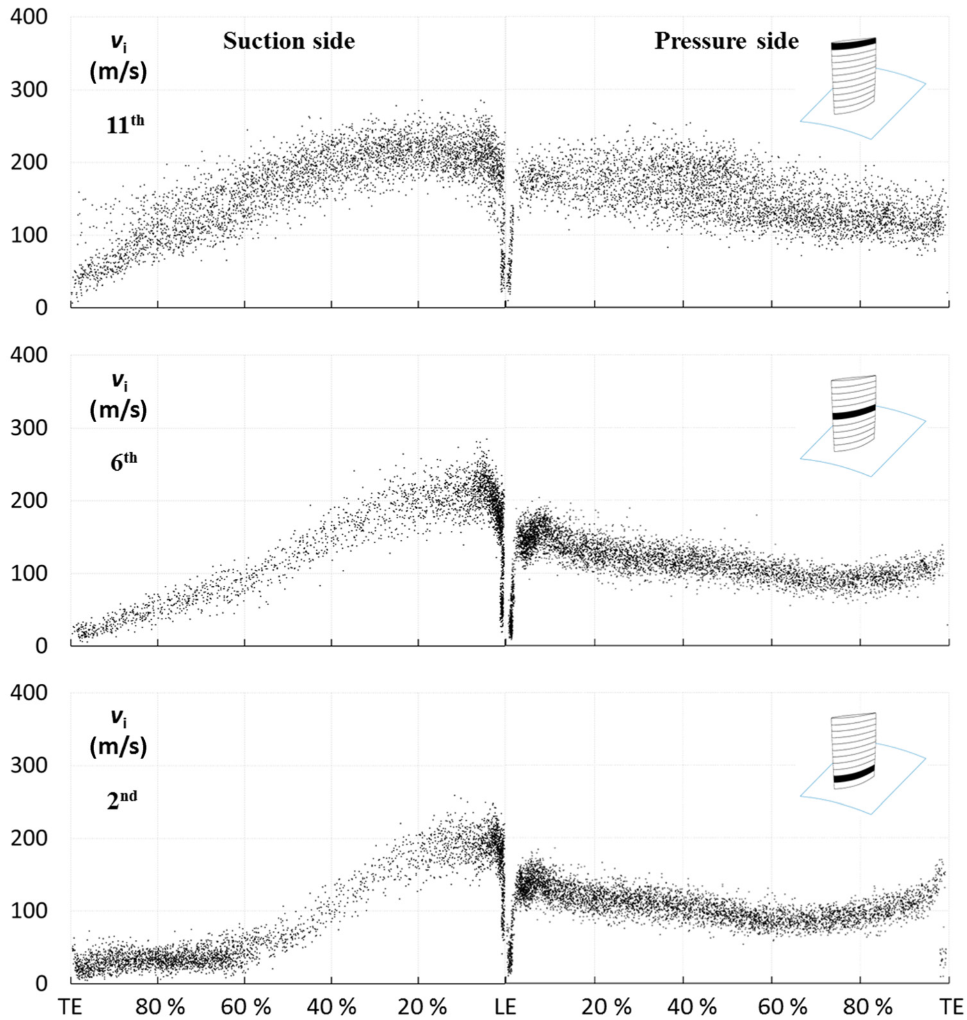

Fig. 7 Impact velocity v_i, second, sixth, and 11th strip, case 1

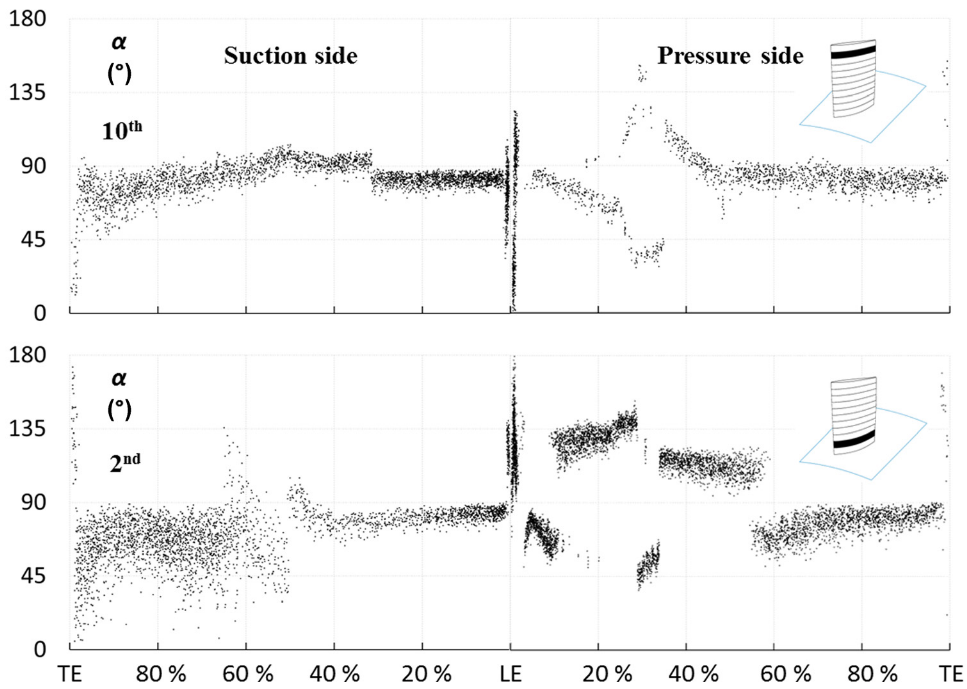

Fig. 8 Impact angle α, second and tenth strip, case 2

but the most important parameters are the normal v_n and tangential v_t velocity components. As in Ref. [6], normal and tangential velocities are calculated for each particle and the angle α is the angle between the surface normal vector and the impact velocity vector.

In Fig. 8, the particle impact angle for the second and tenth strip (case 2) is reported. In some instances the impact angle is higher than 90 deg. This is due to: (i) the surface local curvature (e.g., at the LE and on the TE) and (ii) surface reconstruction approximation during the particle impact postprocess. A deviation can arise from the fact that the surface is reconstructed by interpolating points on the mesh elements in the vicinity of the point of impact. The approximation introduced by this procedure is considered acceptable by the authors, allowing for a confidence band of $\pm$ 5 deg for all the results shown in this paper.

Figure 8 illustrates the following observations:

- The impact angle at the LE assumes different values from 0 deg to 180 deg.
- On the PS the particle impact angle is very close to 90 deg (i.e., the particles are tangential to the blade surface) almost everywhere on the airfoil. A particular area can be noticed in the middle of the chord where the particle impact angle range is wider. This local variation of the impact angle corresponds to the local variation of the blade surface curvature. Thus, it is clearly shown that the local curvature of the airfoil (e.g., dimples, surface damage, etc.) changes the particle impact angle in a significant way and, more generally, the local shape of the blade changes the particle deposition. A different impact angle can determine whether the particle sticks or slips, and thus, the actual shape of the blade surface would determine the magnitude and the rate of the fouling. These findings represent a useful guide for blade surface treatment and control during the manufacturing and maintenance process. The same phenomenon can be noticed for all the strips;
- For the SS, there is also a variation of the particle impact angle in the middle of the chord due to the airfoil curvature. However, it is less noticeable than on the PS.
- On the last part of chord on the SS, the particle impact angle is lower than the PS and this implies that the particle hits the surface with a value of normal velocity which is higher than the tangential velocity. For the second strip, this fact is more evident because the air stream flow is separated from the blade.

Areas characterized at the same time by very high tangential velocity and very low normal velocity (impact angle close to 90 deg) should not be subject to particle deposition because in this case the particles tend to slip on the blade surface. However, in the other areas with a lower impact angle, the normal velocity promotes particle sticking.

As shown in the previous paragraphs, the study of particle adhesion on a surface comprises a large number of aspects and probabilistic analyses are often used due to the unique nature of each contact. In this paper, the authors provide a quantitative analysis of particle adhesion by using the experimental results found in Ref. [12] in which particle velocity and materials are among the most similar to the particles causing fouling phenomena.

SP. With the experimental SP trends reported in Ref. [12], it is possible to define representative trends for the correlation between the normal impact velocity v_n and the SP.

For cases 1, 2, and 3, with a particle diameter in the range of (0.15–0.50) μm the equation for a lower normal impact velocity ($<$ 4 m/s) is

$$S_p = -0.09 v_n + 0.99 \quad (6)$$

while for the higher impact velocity (4–90 m/s) the equation is AQ6

$$S_p = 2 \cdot 10^{-6} v_n^3 - 0.000378\, v_n^2 + 0.011800 v_n + 0.587100 \quad (7)$$

For case 4 with a particle diameter equal to 1.00 μm, the equation for a lower normal impact velocity ($<$ 4 m/s) is

$$S_p = -0.112 v_n + 0.990 \quad (8)$$

while for the higher impact velocity (4–90) m/s the equation is

$$S_p = -6 \cdot 10^{-5} v_n^2 - 6e - 4 v_n + 0.545 \quad (9)$$

With the definition of the SP, for cases 1, 2, and 3 the SP = 0.5 is in correspondence with a normal impact velocity v_n equal to

48.35 m/s. However, for case 4, the SP = 0.5 is in correspondence with a normal impact velocity v_n equal to 22.85 m/s. Thus, the smaller particles have a wider range of normal impact velocity for which the particle impact with the blade surface becomes (with a high probability) a permanent adhesion. Equations (6)–(9) are used to calculate the SP for each particle stuck to the blade surface by using the normal impact velocity.

The particle characteristics used in Ref. [12] are quite different compared to the classic particle characteristics involved in fouling phenomena. In particular, the silicon carbide particles have a very high level of hardness and this implies that the rebound properties could be different from those found in the real fouling applications. Some results related to the influence of the powder hardness on the deposition efficiency are reported in the cold spray deposition studies. A precise complete analysis on this topic could be found in Ref. [24]. The authors report the influence of the powder AQ4 hardness on deposition efficiency. The hardest powder shows the lowest value of deposition efficiency equal to 66% compared to 85% showed by less hard powder.

In Fig. 9, the SP for the second and tenth strips (case 1) is reported. Each dot on the graph represents a particle that hits the blade surface with a normal impact velocity of less than 90 m/s. Only the particles with a normal velocity component toward the surface are taken into account. This procedure allows the identification of the dangerous particles (that will be able to stick) with respect to fouling phenomenon only. Fig. 9 illustrates that:

—The SS is completely covered by particles that have the SP of about 0.8.

—The PS shows an area, in the middle of the airfoil chord, in which the particles have the SP equal to zero. This effect is due to the blade surface curvature mentioned above. For the other regions in the PS, the SP is comparable with the SP on the SS;

—In the regions close to the LE, there are real dispersed values of the SP, probably due to the wide range of the impact angle as reported in Fig. 8.

The other strips show similar features as well as for case 2. As mentioned above, the SP defined in Ref. [12] only considers the normal impact velocity. However, in this application particular attention must be paid to the tangential impact velocity. In fact, as can be seen in Fig. 9, the magnitude of the tangential impact velocity is not negligible.

The tangential impact velocity can reach 200 m/s and 300 m/s in the PS and SS, respectively. These very high values may diminish the SP and could transform the adhesion-impact into the slip-impact. Conversely, it can be noted that in the last part of the airfoil chord on the SS, where the SP is equal to 0.8, the tangential impact velocity is much smaller, thus limiting the possibility of slip between the particle and blade surface. Unfortunately, specific studies on the interaction between the normal impact velocity and the tangential impact velocity are not available in literature and only few studies are reported in the cold spray deposition research field. The authors in Ref. [25] show the influence of the spray angle on the deposition efficiency. The particle approaching angle at which the maximum normal component is equal to the critical velocity is defined as the critical angle. The critical angle is a threshold, less than which no particle deposition occurs. The free of deposition region extends from zero degree to the critical angle. In the transient region, the deposition efficiency increases from 0% to 100%, depending on the velocity of the particles. These angle ranges depend mainly on the ratio of distribution of particle velocity to critical velocity for a given spray material. The maximum deposition region is around the vertical direction and its deposition efficiency reaches nearly 100%.

Specific studies on the variation of the SP due to the presence of a third material at the interface between surface and particle are not available in literature. Generally, in the actual compressors, the presence of a third substance (such as oil, grease, etc.) on the blade surface could increase the SP of the particle. In general, particles that impact on wet surface have more chance to stick there [1], but, at the same time, the droplets that result on the blade surface (due to the humidity and/or to the inlet depression for the early stages) could drag the airborne contaminants from the rotor to the stator surfaces. The influence of the centrifugal forces is well described in Ref. [26] and its greatest "cleaning" effect is well reported in Ref. [27]. In the latter analysis, the salt deposits, generated by the salt carried by the water droplets, are localized in greater quantity on the stator surfaces instead of the rotor surfaces.

In Table 3, all the impact characteristics are reported for cases 1, 2, 3, and 4 which are considered by the authors to be the most interesting cases from a fouling point of view. The particles are subdivided by using normal impact velocity criteria. In particular, the following three categories are defined:

—the particles that move away from the surface (called *Harmless*);

—the particles that have a normal impact velocity less than 90 m/s and for which it can be possible to define an SP by using Eqs. (6)–(9);

—the particles that have an impact normal velocity higher than 90 m/s and for which the SP is assumed equal to zero.

Special attention must be paid to the last category, characterized by an impact normal velocity higher than 90 m/s and an SP equal to zero. These particles possess high kinetic energy that decreases by an order of magnitude during the first impact as reported in Ref. [12]. This phenomenon implies that these particles will not be able to stick during the first contact but instead, it will most likely be during the second one. In fact, the decrease in kinetic energy is strongly related to the decrease in velocity and, consequently, an increase of SP.

Table 3 shows for all categories listed above: (i) the total number of particles N that have impacted on that side (PS or SS) and

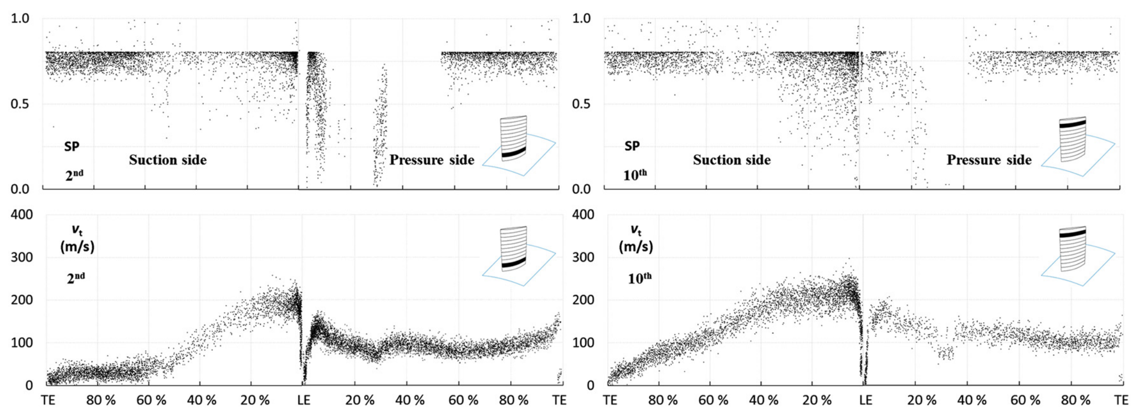

Fig. 9 SP and tangential velocity v_t, second and tenth strip, case 1

Table 3 Particle–blade interaction

		Case 1 ($d_p = 0.15\,\mu m$)				Case 2 (d_p 0.25 μm)				Case 3 ($d_p = 0.50\,\mu m$)				Case 4 ($d_p = 1.00\,\mu m$)			
		PS		SS		PS		SS		PS		SS		PS		SS	
		N	n_{hit} (%)	N	n_{hit} (%]	N	n_{hit} (%)	N	n_{hit} (%)	N	n_{hit} (%)	N	n_{hit} (%)	N	n_{hit} (%)	N	n_{hit} (%)
11^{th}	*Harmless*	690	0.01	1554	0.02	733	0.01	1407	0.02	683	0.01	191	0.00	392	0.00	13	0.00
	$0 < v_n \le 90$ m/s	2887	0.03	2468	0.03	2785	0.03	2406	0.03	3350	0.04	1345	0.02	4426	0.05	19	0.00
	$v_n > 90$ m/s	592	0.01	164	0.00	365	0.00	78	0.00	118	0.00	630	0.01	113	0.00	4391	0.05
	SP ≥ 0.5	2536	0.03	2278	0.03	2515	0.03	2280	0.03	3143	0.04	309	0.00	2286	0.03	11	0.00
10^{th}	*Harmless*	265	0.00	462	0.01	393	0.00	596	0.01	136	0.00	40	0.00	64	0.00	0	0.00
	$0 < v_n \le 90$ m/s	1407	0.02	3277	0.04	1567	0.02	2856	0.03	2788	0.03	2640	0.03	3260	0.04	282	0.00
	$v_n > 90$ m/s	43	0.00	72	0.00	64	0.00	2	0.00	22	0.00	45	0.00	3	0.00	5992	0.07
	SP ≥ 0.5	1346	0.02	3120	0.04	1513	0.02	2830	0.03	2615	0.03	1336	0.02	1009	0.01	5	0.00
9^{th}	*Harmless*	581	0.01	580	0.01	903	0.01	765	0.01	313	0.00	61	0.00	25	0.00	0	0.00
	$0 < v_n \le 90$ m/s	2148	0.03	3956	0.05	2351	0.03	3304	0.04	5270	0.06	3772	0.04	12,161	0.14	3898	0.05
	$v_n > 90$ m/s	92	0.00	34	0.00	107	0.00	0	0.00	26	0.00	0	0.00	4	0.00	0	0.00
	SP ≥ 0.5	2030	0.02	3766	0.04	2271	0.03	3289	0.04	4927	0.06	3437	0.04	603	0.01	334	0.00
8^{th}	*Harmless*	998	0.01	516	0.01	1450	0.02	873	0.01	937	0.01	703	0.01	42	0.00	2	0.00
	$0 < v_n \le 90$ m/s	3241	0.04	3315	0.04	3187	0.04	2675	0.03	5959	0.07	3339	0.04	14,197	0.17	2451	0.03
	$v_n > 90$ m/s	164	0.00	1	0.00	215	0.00	0	0.00	69	0.00	0	0.00	1	0.00	14	0.00
	SP ≥ 0.5	3109	0.04	3236	0.04	3113	0.04	2663	0.03	5858	0.07	3298	0.04	581	0.01	86	0.00
7^{th}	*Harmless*	1187	0.01	383	0.00	1538	0.02	655	0.01	1219	0.01	1578	0.02	168	0.00	15	0.00
	$0 < v_n \le 90$ m/s	3707	0.04	2667	0.03	3637	0.04	2172	0.03	5953	0.07	1371	0.02	12,280	0.15	579	0.01
	$v_n > 90$ m/s	188	0.00	1	0.00	206	0.00	0	0.00	67	0.00	0	0.00	12	0.00	0	0.00
	SP ≥ 0.5	3580	0.04	2604	0.03	3530	0.04	2157	0.03	5856	0.07	1370	0.02	1607	0.02	114	0.00
6^{th}	*Harmless*	1352	0.02	440	0.01	1860	0.02	676	0.01	1596	0.02	2158	0.03	835	0.01	140	0.00
	$0 < v_n \le 90$ m/s	3851	0.04	2443	0.03	3888	0.05	1790	0.02	6579	0.08	336	0.00	7520	0.09	168	0.00
	$v_n > 90$ m/s	123	0.00	8	0.00	117	0.00	1	0.00	38	0.00	0	0.00	20	0.00	0	0.00
	SP ≥ 0.5	3713	0.04	2393	0.03	3710	0.04	1757	0.02	6463	0.08	334	0.00	4286	0.05	136	0.00
5^{th}	*Harmless*	1443	0.02	205	0.00	1937	0.02	222	0.00	1967	0.02	867	0.01	504	0.01	345	0.00
	$0 < v_n \le 90$ m/s	3974	0.05	1906	0.02	3947	0.05	1515	0.02	6781	0.08	53	0.00	5739	0.07	315	0.00
	$v_n > 90$ m/s	95	0.00	6	0.00	76	0.00	4	0.00	23	0.00	0	0.00	14	0.00	0	0.00
	SP ≥ 0.5	3744	0.04	1850	0.02	3648	0.04	1474	0.02	6224	0.07	43	0.00	3804	0.05	315	0.00
4^{th}	*Harmless*	1771	0.02	140	0.00	2327	0.03	129	0.00	2346	0.03	327	0.00	525	0.01	175	0.00
	$0 < v_n \le 90$ m/s	3973	0.05	1778	0.02	4057	0.05	1356	0.02	6492	0.08	49	0.00	7135	0.08	139	0.00
	$v_n > 90$ m/s	64	0.00	7	0.00	52	0.00	5	0.00	58	0.00	0	0.00	326	0.00	0	0.00
	SP ≥ 0.5	3701	0.04	1725	0.02	3692	0.04	1290	0.02	5771	0.07	45	0.00	3062	0.04	139	0.00
3^{rd}	*Harmless*	2027	0.02	235	0.00	2923	0.03	157	0.00	5670	0.07	490	0.01	6541	0.08	498	0.01
	$0 < v_n \le 90$ m/s	3441	0.04	2485	0.03	3175	0.04	2008	0.02	3666	0.04	461	0.01	5382	0.06	552	0.01
	$v_n > 90$ m/s	47	0.00	2	0.00	23	0.00	0	0.00	4	0.00	0	0.00	2	0.00	0	0.00
	SP ≥ 0.5	3054	0.04	2424	0.03	2863	0.03	1964	0.02	3493	0.04	458	0.01	2173	0.03	543	0.01
2^{nd}	*Harmless*	2511	0.03	284	0.00	3293	0.04	256	0.00	6539	0.08	626	0.01	11,566	0.14	482	0.01
	$0 < v_n \le 90$ m/s	2754	0.03	3464	0.04	2718	0.03	3172	0.04	2507	0.03	1914	0.02	2977	0.04	1153	0.01
	$v_n > 90$ m/s	26	0.00	1	0.00	12	0.00	0	0.00	0	0.00	0	0.00	0	0.00	0	0.00
	SP ≥ 0.5	2313	0.03	3429	0.04	2358	0.03	3165	0.04	2357	0.03	1914	0.02	2459	0.03	1003	0.01
1^{ts}	*Harmless*	3518	0.04	1097	0.01	3978	0.05	1607	0.02	6207	0.07	2635	0.03	10,857	0.13	1743	0.02
	$0 < v_n \le 90$ m/s	1911	0.02	3771	0.04	1952	0.02	3657	0.04	1837	0.02	2997	0.03	2562	0.03	3296	0.04
	$v_n > 90$ m/s	8	0.00	315	0.00	8	0.00	0	0.00	46	0.00	0	0.00	0	0.00	0	0.00
	SP ≥ 0.5	1658	0.02	3659	0.04	1699	0.02	3655	0.04	1727	0.02	2991	0.03	1379	0.02	2714	0.03
SIDE	*Harmless*	16,343	0.19	5896	0.07	21,335	0.25	7343	0.09	27,613	0.32	9676	0.11	31,519	0.37	3413	0.04
	$0 < v_n \le 90$ m/s	33,294	0.39	31,530	0.37	33,264	0.39	26,911	0.31	51,182	0.60	18,277	0.21	77,639	0.92	12,852	0.15
	$v_n > 90$ m/s	1442	0.02	611	0.01	1245	0.01	90	0.00	471	0.01	675	0.01	495	0.01	10,397	0.12
	SP ≥ 0.5	30,784	0.36	30,484	0.36	30,912	0.36	26,524	0.31	48,434	0.57	15,535	0.18	23,249	0.28	5400	0.06

on that strip (1st–11th) and (ii) the ratio n_{hit} between the total number N and the number of injected particles. Thus, the ratio n_{hit} shows a global overview, in line with the fouling susceptibility criteria that consists of the ratio between the number of stuck particles and the total number of particles injected into the flow path. In Table 3 N and n_{hit} related to the particles characterized by an SP equal to or greater than 0.5 are also reported. Finally, the rows grouped by the name SIDE contain the sum of the values reported for each strip. With this global overview, it is possible to highlight the different behaviors of particle deposition on the blade surface:

—The percentages of the particles with $v_n > 90$ m/s are higher for the strips close to the tip, especially in the SS, for all cases. This phenomenon is the precursor to the erosive effects that are produced by the particles with a diameter greater than 10 μm, as reported in Ref. [17]. In fact, the normal impact velocity increases with the increase of the particle diameter and, in the same way, the particles become less able to stick, although the impact is more dangerous for the blade surface. In the other strips, the number of particles with an impact normal velocity higher than 90 m/s is almost negligible.

—In the SS, the number of particles with SP > 0.5 decreases with an increase of particle diameter, while in the PS, this number remains in the same order of magnitude for all cases.

—The *Harmless* particles are present in a great quantity in the strips close to the hub. This fact highlights that the percentage of dangerous particles (from a fouling point of view) is higher at the top of the blade.

With the spanwise subdivision of the results shown in Table 3, we can underline the difference in terms of particle–blade interaction behavior between the SS and PS. In particular, the presence of the dangerous particles at the top of the blade could be responsible for a greater compressor performance drop. As reported by Aldi et al. [28], the effects of fouling at the blade tip (e.g., the increase in surface roughness) have a greater influence on the compressor performance degradation. The localization of the deposit on the blade represents a key aspect in the fouling phenomenon. As already mentioned for the deposits on the blade tip, the difference in the deposits between PS and suction is also important. As pointed out by Morini et al. [29], the effects of fouling on the SS (e.g., the increase in surface roughness) have a greater influence on the compressor performance degradation.

Figure 10 reports the trend of the ratio $n_{hit,SP>0.5}$ (black continuous line) for the particles with SP > 0.5 superimposed with the trend of the η_{hit} (gray dotted line). The two trends refer to both sides of the blade (PS and SS).

As mentioned above, η_{hit} represents the fouling susceptibility and its values represent a key result for gas turbine operators.

As can be seen from Fig. 10, for the PS the trend of $n_{hit,PS,SP>0.5}$ does not follow the trend of $\eta_{hit,PS}$ unlike the trends reported for the SS. For the PS, the number of stuck particles is quite independent to the total number of particles that hit the blade and the $n_{hit,PS,SP>0.5}$ remains almost the same for the four considered cases. In this case, the higher particles produce more fouling effects due to their higher diameter and thus higher mass. For the SS, the ratio $n_{hit,SS,SP>0.5}$ shows a very high percentage of particles able to stick for the smallest diameters compared to the total number of particles that hit the SS.

The greater tendency of particles to stick to the SS is an important result and focuses attention not only on the quantity of ingested contaminants but also on the fluid dynamic phenomena that characterize the flow around the blade. On the SS, case 1 is the most severe from a fouling point of view. The particles arrive with a normal impact velocity that makes it extremely effective in sticking to the blade surface.

The deposits on the SS have the highest influence on the axial compressor performance drop, and for this reason, the filtration system must be designed to remove the smaller particles (up to 0.5 μm) from the airflow stream because the bigger particles are not able to reach the SS due to their inertia. In contrast, in the PS, the particles that could stick do not determine a great performance drop and these deposits could be removed by proper periodic washing operations. Thanks to this evidence, water droplets must only clean the PS. The deposits on the LE, due to the airfoil nose, are easily removed through the washing operation. As reported by Day et al. [30], all diameter droplets (diameters in the range 50–200 μm) surround the LE easily.

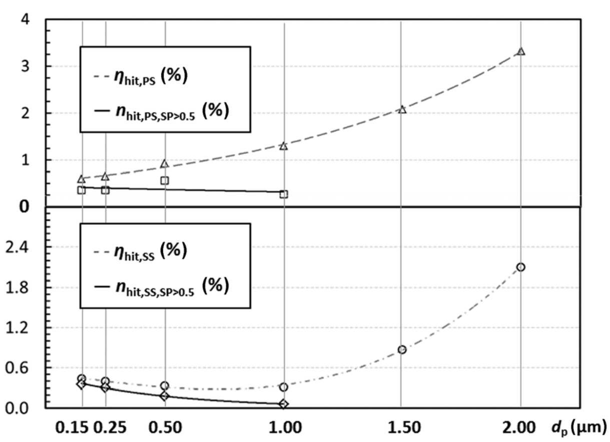

Fig. 10 Trends of the ratio $n_{hit,SP>0.5}$ and η_{hit} superimposed

Comparison: Subsonic Versus Transonic Rotor

As mentioned above, the study of particle impact/adhesion presented in this paper for a subsonic rotor, is the continuation of a previous work conducted for a transonic rotor [5,6]. In this section, the authors report a comparison between the two studies. The comparison is presented in qualitative form and represents an easy-to-use statement of the particle impact/adhesion in axial compressors.

The comparison related to particle impact behavior can be summarized as follows:

—For both rotors, the percentage of the particles that hit the blade surface increases with the diameter of the particles but the transonic rotor is more affected by the particle impact (the mass flow rates swallowed by the two rotors are in the same order of magnitude as well as the amount of the contaminant).

—For both rotors, by increasing particle diameter, the PS is more affected by the impacts, thus the particles tend to hit the PS in increasing quantities as the particle diameter increases.

—For the SS, by increasing the particle diameter the SS is less affected by the impacts in case of transonic rotor, while in the case of the subsonic rotor, by increasing the particle diameter, the number of particles that hit the blade decreases to $d_p = 1.00\,\mu$m, while the number of impacts that take place on the SS increases from $d_p = 1.00\,\mu$m to $d_p = 2.00\,\mu$m. For these reasons, the subsonic rotor shows a more distributed particle impact pattern.

—The maximum value of the fouling index is an order of magnitude higher in the case of the transonic rotor (3.09 compared to 0.39 for the subsonic rotor).

—The major differences in the particle impact pattern between the rotors are localized in the LE zone. The particles can surround the subsonic LE (from PS to SS) because it is thicker than the transonic LE while, in the case of the transonic rotor, the thinner LE allows particle impact only in the PS.

The comparison related to particle adhesion behavior can be summarized as follows:

—The particle impact velocity is lower in the case of the subsonic rotor due to the lower peripheral velocity. This implies that the impacting particles on the subsonic blade have a greater probability of sticking because the SP is related to the normal impact velocity magnitude;

—The flow separation in the SS influences the particle adhesion in both rotors. In particular, the separation reduces the magnitude of the air velocity field around the blade and this implies that the particle impact velocity became smaller determining the aforementioned effect.

—The trend of the percentage of the particles that could stick in the pressure side ($n_{hit,PS,SP>0.5}$) for the transonic rotor are almost independent with respect to the particle while, in the case of the subsonic rotor, this percentage decreases with the particle diameter. Thus, the bigger particles that impact in the PS are more dangerous in the case of the transonic rotor.

—The trend of the percentage of particles that could stick in the suction side ($n_{hit,SS,SP>0.5}$) follow the trend of the capture efficiency in both rotors.

In general, it is not possible to define which compressor is more sensitive to the fouling issue because the smallest capture efficiency value shows by the subsonic rotor must be compared to the smallest value of the particle impact velocity that leads to a higher value of SP.

Conclusions

In this paper, an extended study on microparticle ingestion and adhesion on the axial compressor blade surface was carried out. The adopted numerical and postprocess strategies have been presented and validated in a previous work. Using realistic air contamination data, the filtration efficiency of state-of-the art air filtration systems and the size of the axial compressor, we obtained results for both the particle trajectories and the magnitude of fouling which can afflict the axial compressor.

The results of the particle impacts have shown that: (i) the percentage of particles that hit the blade surface increases with the diameter of the particles and (ii) with the increasing particle diameter the PS is more affected by the impacts. For the SS, the trend is more complex due to the shape of the airfoil nose. The biggest particles that impact in the SS are concentrated only on the first part of the airfoil chord.

Regarding particle deposition, the most important results refer to the relationship between the particle diameter and the percentage of stuck particles. On the SS, the smaller particles are the most numerous from a fouling point of view due to the high total number of particles characterized by an SP greater than 0.5. In the SS the combined effects of the SP values and impact tangential velocity determine the most dangerous fouling conditions.

From these results, some guidelines related to the management of gas turbine installations were pointed out. The results of this study highlight the advantage of installing air filtration systems that can remove small and very small particles from the air stream. This would allow the use of effective online washing using larger droplets that would typically only hit and clean the PS of the blade.

Comparing the results obtained in the previous work for a transonic rotor with the results presented in this paper, the difference between the two rotors focused on the number of particles that

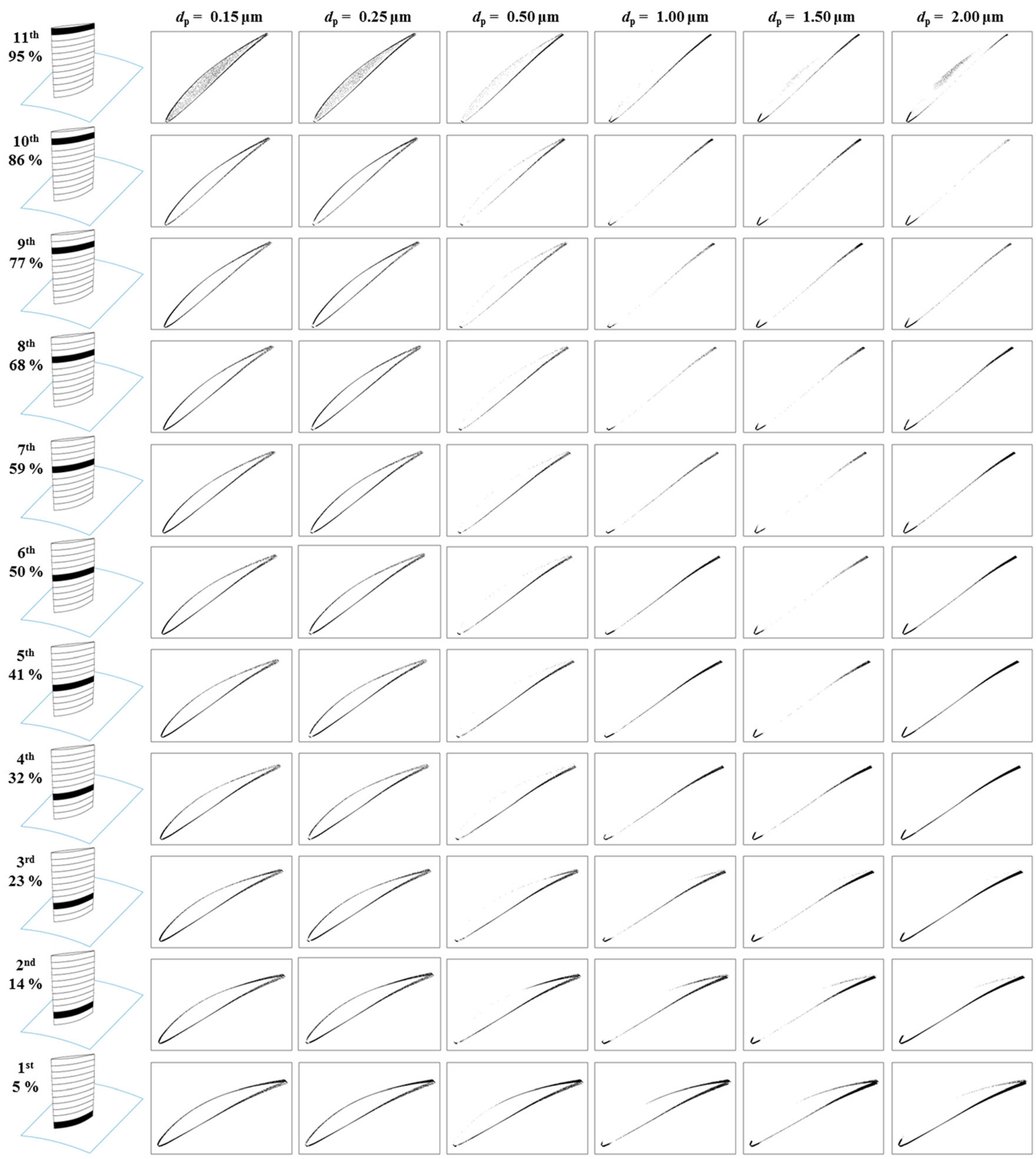

Fig. 11 Spanwise subdivision (left side) and overall impact patterns

impact the blade and the particle impact velocity magnitude. For both quantities, the subsonic rotor showed a smaller value, and a priori, it is not possible to define which compressor is more sensitive to the fouling issue.

Future studies would have to analyze the behavior of a multistage axial compressor, in particular the change in the particle deposition along the stage and the effects of only water washing. An increase in the knowledge of fouling through the use of numerical codes may therefore constitute a decisive element for better planning of maintenance of turbomachinery.

Nomenclature

A = area
b = bounce (average)
d = diameter
H = fouling index
m = mass flow rate
M = mass
n = ratio
N = total particles (referred to particles)
p = pressure
q = volume flow rate
St = Stokes number
u_t = shear velocity
v = relative velocity particle
X = impact concentration (blade)
$y+$ = nondimensional distance

Greek Symbols

α = impact angle
β = compression ratio
ε = dissipation rate of turbulent kinetic energy
η = efficiency
k = turbulent kinetic energy
μ = dynamic viscosity
ν = kinematic viscosity
ρ = density
τ = shear stress
$\tau+$ = nondimensional particle relaxation time
χ = particle concentration (air)

Subscripts and superscripts

b = bounce
f = filtration system
h = hydraulic
hit = hit (referred to particle–blade interaction)
i = impact
n = normal direction
p = particle
side = side (referred to the side of the blade)
SLICE = slice (referred to chordwise division)
t = tangential direction
TT = total-to-total
w = wall
1 = inlet
2 = outlet
- = average

Acronyms

DPM = discrete phase model
DRW = discrete random walk
CFD = computational fluid dynamics
LE = leading edge
PS = pressure side
SEM = scanning electron microscope
SP = sticking probability
SS = suction side
STW = standard wall function
TE = trailing edge

Appendix

Overall Impact Patterns

All the particle impact patterns in Fig. 11 are reported. Each pattern represents the projection of the fouled airfoil into a perpendicular plane with respect to the spanwise direction. On the left side, the spanwise station and the correspondent percentage of the blade span can be seen. The blade was divided by 11 strips along the spanwise direction and each dot on the graph represents a single particle that has hit the blade surface. The upper surface is the SS, while the lower surface is the PS, for each picture.

References

[1] Kurz, R., and Brun, K., 2012, "Fouling Mechanism in Axial Compressors," ASME J. Eng. Gas Turbines Power, **134**(3), p. 032401.
[2] Kurz, R., Brun, K., Meher-Homji, C., and Moore, J., 2012, "Gas Turbine Performance and Maintenance," 41st Turbomachinery Symposium, Sept. 24–27, Houston, TX.
[3] Wilcox, M., Baldwin, R., Garcia-Hernandez, A., and Brun, K., 2010, *Guideline for Gas Turbine Inlet Air Filtration Systems*, Release 1.0, ■, ■. AQ5
[4] Vigueras Zuniga, M. O., 2007, "Analysis of Gas Turbine Compressor Fouling and Washing on Line," Ph.D. thesis, Cranfield University, Cranfield, Bedfordshire, UK.
[5] Suman, A., Kurz, R., Aldi, N., Morini, M., Brun, K., Pinelli, M., and Spina, P. R., 2014, "Quantitative CFD Analyses of Particle Deposition on a Transonic Axial Compressor Blade, Part I—Particle Zones Impact," ASME J. Turbomach., **137**(2), p. 021009.
[6] Suman, A., Morini, M., Kurz, R., Aldi, N., Brun, K., Pinelli, M., and Spina, P. R., 2014, "Quantitative CFD Analyses of Particle Deposition on a Transonic Axial Compressor Blade, Part II—Impact Kinematics and Particle Sticking Analysis," ASME J. Turbomach., **137**(2), p. 021010.
[7] Hertz, H., 1896, *Miscellaneous Papers*, Macmillan and Co., Ltd., London, UK (Authorised English Translation), pp. 146–183.
[8] Johnson, K. L., Kendall, K., and Roberts, A. D., 1971, "Surface Energy and the Contact of Elastic Solids," Proc. R. Soc. London. Ser. A, **324**(1558), pp. 301–313.
[9] Wall, S., John, W., Wang, H. C., and Goren, S. L., 1990, "Measurements of Kinetic Energy Loss for Particles Impacting Surfaces," Aerosol Sci. Technol., **12**(4), pp. 926–946.
[10] Thornton, C., and Ning, Z., 1998, "A Theoretical Model for the Stick/Bounce Behavior of Adhesive Elastic–Plastic Spheres," Powder Techonol., **99**(2), pp. 154–162.
[11] Parker, G. J., and Lee, P., 1972, "Studies of the Deposition of Sub-Micron Particles on Turbine Blades," Proc. Inst. Mech. Eng., **186**(1), pp. 519–526.
[12] Poppe, T., Blum, J., and Henning, T., 2000, "Analogous Experiments on the Stickiness of Micron-Sized Preplanetary Dust," Astrophys. J., **533**(1), pp. 454–471.
[13] Poppe, T., and Blum, J., 1997, "Experimental on Pre-Planetary Grain Growth," Adv. Space Res., **20**(8), pp. 1595–1604.
[14] Palomba, E., Poppe, T., Colangeli, L., Palumbo, P., Perrin, J. M., Bussoletti, E., and Henning, T., 2001, "The Sticking Efficiency of Quartz Crystals for Cosmic Sub-Micron Grain Collection," Planet. Space Sci., **49**(9), pp. 919–926.
[15] Suzuki, M., Inaba, K., and Yamamoto, M., 2008, "Numerical Simulation of Sand Erosion Phenomena in Rotor/Stator Interaction of Compressor," J. Therm. Sci., **17**(2), pp. 125–133. AQ8
[16] Suzuki, M., and Yamamoto, M., 2011, "Numerical Simulation of Sand Erosion Phenomena in a Single-Stage Axial Compressor," J. Fluid Sci. Technol., **6**(1), pp. 98–113.
[17] Ghenaiet, A., 2012, "Study of Sand Particle Trajectories and Erosion Into the First Compression Stage of a Turbofan," ASME J. Turbomach., **134**(5), p. 051025
[18] Ahlert, K., 1994, "Effects of Particle Impingement Angle and Surface Wetting on Solid Particle Erosion of AISI 1018 Steel," M.S. thesis, Department of Mechanical Engineering, The University of Tulsa, Tulsa, OK.
[19] Forder, A., Thew, M., and Harrison, D., 1998, "A Numerical Investigation of Solid Particle Erosion Experienced Within Oilfield Control Valves," Wear, **216**(2), pp. 184–193.
[20] Zohdi, T. I., 2005, "Modeling and Direct Simulation of Near-Field Granular Flows," Int. J. Solid Struct., **42**(2), pp. 539–564. AQ7
[21] Tian, T., and Ahmadi, G., 2006, "Particle Deposition in Turbulent Duct Flows—Comparisons of Different Model Predictions," J. Aerosol Sci., **38**(4), pp. 377–397.
[22] Fottner, L., 1989, "Review of Turbomachinery Blading Design Problems," Report No. AGARD-LS-167.
[23] Gbadebo, S. A., Cumpsty, N. A., and Hynes, T. P., 2005, "Three-Dimensional Separations in Axial Compressors," ASME J. Turbomach., **127**(2), pp. 331–339.

[24] Papyrin, A. N., Kosarev, V. F., Klinkov, S., Alkhimov, A. P., and Fomin, V., 2007, *Cold Spray Technology*, Elsevier, Oxford, UK.
[25] Li, C. J., Li, W. Y., Wang, Y. Y., Yang, G. J., and Fukanuma, H., 2005, "A Theoretical Model for Prediction of Deposition Efficiency in Cold Spraying," Thin Solid Films, **489**(1–2), pp. 79–85.
[26] Tarabrin, W. P., Schurovsky, V. A., Bodrov, A. I., and Stalder, J.-P., 1998, "Influence of Axial Compressor Fouling on Gas Turbine Unit Performance Based on Different Schemes and With Different Initial Parameters," ASME Paper No. 98-GT-416
[27] Syverud, E., Brekke, O., and Bakken, L. E., 2005, "Axial Compressor Deterioration Caused by Saltwater Ingestion," ASME Paper No. GT2005-68701.
[28] Aldi, N., Morini, M., Pinelli, M., Spina, P. R., Suman, A., and Venturini, M., 2014, "Performance Evaluation of Non-Uniformly Fouled Axial Compressor Stages by Means of Computational Fluid Dynamics Analyses," ASME J. Turbomach., **136**(2), p. 021016.
[29] Morini, M., Pinelli, M., Spina, P. R., and Venturini, M., 2011, "Numerical Analysis of the Effects of Non-Uniform Surface Roughness on Compressor Stage Performance," ASME J. Eng. Gas Turbines Power, **133**(7), p. 072402.
[30] Day, I., Williams, J., and Freeman, C., 2008, "Rain Ingestion in Axial Flow Compressors at Part Speed," ASME J. Turbomach., **130**(1), p. 011024.